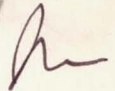


File 54T 204-1-16-1  
264  


**NASA TECHNICAL  
MEMORANDUM**

NASA TM X-73575

NASA TM X-73575

**PREDICTION OF LAMINAR AND TURBULENT BOUNDARY  
LAYER FLOW SEPARATION IN V/STOL ENGINE INLETS**

by D. C. Chou, R. W. Luidens, and N. O. Stockman  
Lewis Research Center  
Cleveland, Ohio 44135

TECHNICAL PAPER to be presented at the  
Fifteenth Aerospace Sciences Conference sponsored by the  
American Institute of Aeronautics and Astronautics  
Los Angeles, California, January 24-26, 1977

PREDICTION OF LAMINAR AND TURBULENT BOUNDARY LAYER

FLOW SEPARATION IN V/STOL ENGINE INLETS

by D. C. Chou,\* R. W. Luidens, N. O. Stockman

Lewis Research Center

ABSTRACT

The paper provides a theoretical description of the development of the boundary layer on the lip and diffuser surface of a subsonic inlet at arbitrary operating conditions of mass flow rate, freestream velocity and incidence angle. Both laminar separation on the lip and turbulent separation in the diffuser are discussed. The agreement of the theoretical results with model experimental data illustrates the capability of the theory to predict separation. The effects of throat Mach number, inlet size, and surface roughness on boundary-layer development and separation are illustrated.

INTRODUCTION

Many proposed advanced aircraft, whether CTOL, STOL or VTOL, require propulsion system inlets to operate over wide ranges of flight speed, incidence angle and inlet throat Mach numbers (weight flow rates). A major design criterion for these types of inlets is that internal flow separation be avoided, particularly separation of the type that can cause unacceptable total pressure loss or distortion. This requirement can be quite severe for a fixed-geometry axisymmetric inlet. Therefore, considerable research and development effort is required for the design of such inlets.

The principal tool in inlet design has been wind tunnel experiments with scale model inlets. Wind tunnel testing is both time consuming and expensive. Furthermore, applying scale model data to the design of full scale inlets may result in unnecessarily conservative designs. For these reasons a reliable theoretical method of predicting internal flow separation is desirable.

The NASA-Lewis Research Center is currently in the process of developing such a method. It consists of a series of computer programs that calculate the potential and viscous flow, including separation prediction, in arbitrary inlets. Recent status reports on these programs are given in references 1 and 2.

---

\* Present position, University of Iowa.

These programs were used to conduct a thorough investigation of the boundary layer development around the lip and diffuser surface of an inlet designed for the Quiet Clean Short Haul Experimental Engine (QCSEE). The present paper presents some results from that investigation.

Included are comparisons of theoretical with experimental separation bounds; some effects of varying the inlet operating conditions on the boundary layer behavior; and a discussion of both lip and diffuser separation, and the stability of diffuser separation.

The boundary layer development is illustrated in detail for a typical set of operating conditions. Finally the effects of surface roughness and of model scale (up to full size) are discussed.

#### NOMENCLATURE (see also fig. 1)

$C_f$	local skin friction coefficient (ratio of wall shear stress to dynamic pressure at edge of boundary layer)
$D_e$	diffuser exit diameter, cm
$H$	shape factor, ratio of boundary layer displacement to momentum thickness
$M$	local Mach number
$M_T$	average one-dimensional throat Mach number based on inlet weight flow rate and geometric throat area
$M_o$	free stream Mach number
$S$	surface distance from inlet highlight
$u/U$	ratio of velocity in the boundary layer to velocity at the edge of the boundary layer
$y$	distance in the boundary layer normal to the inlet surface, cm
$\alpha$	inlet incidence angle, deg.
$\delta$	boundary layer thickness, cm

#### Experimental Background

The inlet geometry chosen for the present study is shown in figure 1. Pertinent geometric parameters and terminology are indicated on the figure.



This inlet was chosen because its experimental separation bounds had been determined from tests in the Lewis Research Center 9x15 foot low speed wind tunnel.

The experimental separation bounds, taken from reference 3, are shown in figure 2 on a plot of incidence angle  $\alpha$  versus average throat Mach number for two values of free stream Mach number. These data were obtained by setting the free stream Mach and the throat Mach number (weight flow rate) and then increasing the inlet incidence angle to the point of observed lip separation. The angles used to generate the separation bounds shown on the figure are the angles just before the flow separates. The separation bounds appeared as bands rather than lines because of scatter in the data.

As illustrated in figure 3, if the incidence angle is increased just beyond the separation bound, separation occurs and the throat Mach number (weight flow) drops. This dropping of weight flow is observed experimentally at all throat Mach numbers and is illustrated on figure 3 for the lower throat Mach number range.

#### CALCULATION PROCEDURE

The major elements of the overall computing system are described in references 1 and 2 and the details of the boundary layer calculations are given in references 4 and 5. The calculation procedure consists of five major steps: (1) inlet geometry definition; (2) calculation of incompressible potential flow basic solutions; (3) combination of basic solutions into a solution satisfying arbitrary operating conditions of inlet mass flow, free stream velocity and inlet angle-of-attack; (4) correction of the incompressible flow for compressibility; and (5) calculation of boundary layer using the surface Mach number distribution obtained in step (4).

The boundary layer program calculates boundary layer velocity profiles, displacement thickness  $\delta^*$ , skin friction coefficient  $C_f$ , etc. at each station. The boundary-layer calculation proceeds from laminar flow (at the stagnation point) through transition into turbulent flow. Transition is predicted based on the empirical correlations of reference 6. Flow separation is indicated by zero wall shear stress, i.e., when the local skin friction coefficient is zero.

The boundary layer calculations are based on the assumption that the flow is axisymmetric. Thus, any secondary flow due to the inlet being at non-zero angle-of-attack is neglected.

There are additional shortcomings of the boundary-layer calculation. Many inlets of current interest, including the QCSEE inlet investigated

herein, contain regions of local supersonic flow. Thus, there is the possibility of shock-boundary-layer interaction which the present analysis does not account for. Also, the transition model does not account for the separation bubbles that are evident in some of the inlet surface static pressure distributions. In spite of these shortcomings, generally good agreement has been obtained with experimental data (e.g. ref. 7).

## RESULTS AND DISCUSSION

Theoretical results are presented for the inlet of figure 1 at two values of free stream Mach number and a range of values of throat Mach number and inlet incidence angle. At both free stream Mach numbers, predicted and experimental separation bounds are compared. For one typical case, the boundary layer development is given in some detail. Finally, the effects of surface roughness and model scale are illustrated.

### Free Stream Mach Number of 0.12

The effect of incidence angle on two important flow parameters on the inlet windward internal surface is shown in figure 4 as a function of the surface distance from the inlet highlight for a throat Mach number of 0.59. Three values of incidence angle were selected to illustrate attached flow ( $56^\circ$ ), diffuser separation ( $64^\circ$ ), and lip separation ( $92^\circ$ ).

Figure 4(a) shows the local surface Mach number distribution from the stagnation point ( $M=0$ ) to the diffuser exit ( $S/D_e \approx 1.0$ ). Note that increasing the incidence angle produces two effects unfavorable to maintaining attached flow: (1) it increases the peak Mach number near the highlight ( $S/D_e = 0$ ) and consequently the diffusion required to the diffuser exit; and (2) it moves the stagnation point ( $M=0$ ) further around on the outside of the inlet (increasing negative values of  $S/D_e$ ) thus increasing the boundary layer buildup ahead of the peak Mach number.

The corresponding local skin friction coefficient distributions are shown in figure 4(b). The criterion for boundary layer separation is that the skin friction coefficient  $C_f$  go to zero. Separation onset is defined to occur when  $C_f = 0$  and  $dC_f/dS = 0$  as illustrated in the figure. It is the 'separation onset' that is plotted in the subsequent figures. Its value is usually estimated from calculations that fall on both sides of the onset. It can be seen from figure 4(b) that for  $\alpha = 56^\circ$  the flow does not separate but that two areas for potential separation exist. They are the minimum  $C_f$  points, one in the diffuser and one on the lip. An increase in incidence angle to  $64^\circ$  causes  $C_f$  to go to zero in the diffuser,  $S/D_e = 0.6$  indicating diffuser separation at this flow condition. A further increase in  $\alpha$  to  $92^\circ$  causes  $C_f$  to go to zero on the lip indicating lip separation. Note that diffuser separation is in the fully turbulent region and lip separation is at the



beginning of the transition region and is essentially laminar separation.

The calculations that produced figure 4 can be repeated at several values of average throat Mach number  $M_T$  and a range of values of incidence angle  $\alpha$  to determine separation onset incidence angle. The results can then be used to generate the separation onset curves shown in figure 5. The flow is attached below the curves and separated above the curves. There are two theoretical separation onset curves in the figure: one for diffuser separation and the other for lip separation. The experimental separation onset data are also shown on the figure. In all cases when the experimental separation was observed, it was from the inlet lip. However, the instrumentation was not capable of telling if the separation had initiated in the diffuser and then propagated rapidly upstream to the lip. This possibility will be considered in more detail in the discussions of this and several following figures.

As was noted in the experimental results presented in figure 3, when separation occurs the weight flow (and thus  $M_T$ ) drops. It is hypothesized that if separation starts in the diffuser, the weight flow decreases continuously with the upstream movement of the separation point. Now consider the theoretical diffuser separation onset curve. It has a maximum at an  $M_T$  of about 0.6. To the right of this maximum if separation occurs, the weight flow drops moving the inlet operating point to the left into the attached-flow region. Thus, to the right of the maximum, diffuser separation is stable that is, it does not propagate upstream to the lip. However, if the incidence angle is increased sufficiently, the theory predicts the onset of lip separation. The predicted lip separation agrees reasonably well with the experimentally observed separation which is also from the lip.

On the other hand, to the left of the maximum of the theoretical diffuser separation onset curve; ( $M_T < 0.6$ ), when diffuser separation occurs with the concomitant weight flow drop, the inlet operating point moves deeper into the separated region. Thus to the left of the maximum diffuser separation is unstable, that is, it does propagate upstream to the lip. This type of separation is then observed in the experiment as occurring at the lip. With this interpretation, the theory and data agree.

Thus, for this inlet, the rules for interpreting analytical results for predicting the separation which will be observed experimentally as occurring from the inlet lip are: if the throat Mach number,  $M_T$ , is to the left of the maximum of the theoretical diffuser separation onset curve, the calculated diffuser separation angle is interpreted as the predicted lip separation angle; if the throat Mach number is to the right of the maximum of the theoretical diffuser separation onset curve, the theoretical lip separation angle is also the predicted lip separation angle.

The stable and unstable regions of diffuser separation can also be illustrated theoretically. Figure 6(a) is a plot of local skin friction coefficient versus surface distance in the inlet for  $\alpha = 56^\circ$  for several

values of throat Mach number (weight flow) in the unstable region ( $M_T < 0.6$ ). The reference curve is from a case of attached flow with  $M_T = 0.59$ . Reducing throat Mach number to 0.46 causes the flow to separate at an  $S/D_e$  of about 0.6. It is hypothesized that this separation causes a reduction in average throat Mach number. Reduction of throat Mach number (to 0.28, for example) moves the separation point further upstream producing a greater extent of separated flow and reducing the weight flow still further. This process can continue until the separation reaches the lip.

On the other hand, figure 6(b) shows the affect of reducing the weight flow in the stable region. Starting with a throat Mach number,  $M_T$ , of 0.78, the flow is separated which should reduce the average throat Mach number. Decreasing throat Mach number  $M_T$  to 0.70 causes the flow to become attached; reducing throat Mach number  $M_T$  further to 0.59 moves the flow even further from separation. Thus a diffuser separation at these higher throat Mach numbers will not only not propagate upstream but the flow will tend to become attached when the weight flow drops due to diffuser separation.

The Mach number distributions for all the cases of figure 6(a) and (b) are shown on figure 6(c). Note that there appears to be no obvious way of predicting whether a given case will separate or not by looking at the Mach number distribution. Even comparing a given Mach number distribution to one that is known to be attached or separated does not aid in prediction of the boundary layer behavior.

#### Free Stream Mach Number of 0.18

Plots comparable to those of the previous section for a higher free stream Mach number of 0.18 (65 m/sec, 126 knots) are presented in figure 7. Figure 7(a) shows the effect on the local surface Mach number of varying the incidence angle at or near separation for a high throat Mach number of 0.73. The shapes of the Mach number distributions do not differ greatly from those of figure 4(a); however, the incidence angle at which a given peak Mach number occurs is lower for the higher freestream Mach number case. Also, the angles at which diffuser and lip separation occur are lower here than for the  $M_o = 0.12$  case of figure 4(a). The skin friction coefficient distributions are shown on figure 7(b) for the corresponding Mach number distributions of figure 7(a). As before, this plot shows the location of the predicted separation point for each value of  $\alpha$ : no separation at  $\alpha = 44^\circ$ , diffuser separation at  $50^\circ$  and lip separation at  $54^\circ$ .

Similarly, separation angles were found for other values of  $M_T$  and the resulting separation onset curves are shown in figure 8 along with the experimental data for  $M_o = 0.18$ . Once again, as in figure 5, the theoretical diffuser separation curve agrees with the experimental curve (where separation is observed to occur from the lip) to the left of the



probable diffuser separation curve peak. To the right of this peak, there is little difference between the predicted lip and diffuser separation onset curves and both are in reasonable agreement with the experimental data. Thus, the same interpretation of the theoretical results used to predict the observed experimental separation bounds at  $M_o = 0.12$ , (fig. 5) also applies here for  $M_o = 0.18$ .

The effect of average throat Mach number on local flow conditions at  $\alpha = 44^\circ$  is shown in figure 9. The local Mach number distributions (fig. 9(a)) indicate as before that there is no obvious way of predicting from the Mach number distribution alone whether the inlet will separate or not. The corresponding skin friction distributions are shown in figure 9(b), and again show the separation point moving upstream as the throat Mach number (weight flow rate) is decreased.

#### Boundary Layer Details

Figure 10 shows the local skin friction coefficient and shape factor distributions and also boundary layer profile shapes and thickness at selected locations for a typical attached-flow case. (The Mach number distributions corresponding to this case ( $M_T = 0.80$ ,  $M_o = 0.18$ ,  $\alpha = 44^\circ$ ) is given on fig. 9(a)).

For comparison with the values of shape factors shown, the values for a flat plate are 2.6 for a laminar boundary layer and 1.3 for a turbulent boundary layer.

Upstream of the highlight ( $S/D_e < 0$ ) the boundary layer is thin and laminar, and the shape factor and velocity profile shown are representative of laminar flow. At the start of the transition region, there is a sharp increase in shape factor corresponding to a sharp drop in local skin friction coefficient and increase in the Mach number (fig. 9(a)), i.e. in a very favorable pressure gradient. The shape factor reaches a peak value of 4.4 approximately where the skin friction reaches a minimum, both indications of a tendency to separation. Correspondingly, it can be judged from the shape of the dimensionless boundary layer profile that the velocity gradient at the wall  $d(u/U_o)/d(y/\delta)$  has decreased; a value of zero would, of course, indicate separation.

In the transition region as the boundary layer becomes fully turbulent, the shape factor decreases rapidly, the skin friction coefficient increases, and the boundary layer thickness  $\delta/D_e$  continues to increase. The profile is fuller,  $d(u/U_o)/d(y/\delta)$  has increased, so the boundary layer has moved away from separation.

Midway down the diffuser,  $S/D \approx 0.7$ , the turbulent boundary layer parameters all show a tendency to separation; namely an increasing shape factor, a skin friction coefficient approaching zero and a retarded boundary layer profile. Toward the end of the diffuser the boundary layer recovers



a healthier set of characteristics.

Figure 10 has illustrated some of the details in the boundary layer typical of those for all the preceeding results. For all those cases the surface was assumed to be smooth and scale corresponds to diffuser exit diameter,  $D_e$ , of 30.6 cm (12"). The following sections discuss the effect of surface roughness and scale.

#### Effect of Surface Roughness

The boundary layer program accounts for the surface roughness through the input of the Nikuradse sand roughness (ref. 8). To investigate this effect on the boundary layer development several values of Nikuradse sand roughness were considered. Although the program can handle roughness varying over the surface, for this study the roughness was constant over the entire surface for each case. Figure 11 shows the skin friction coefficient distribution for several values of roughness from zero (smooth wall) to 0.013 cm (0.005 in.). The inlet operating conditions ( $M_T = 0.73$ ,  $M_O = 0.18$ ,  $\alpha = 44^\circ$ ) were chosen so that the smooth wall case was very close to diffuser separation. It can be seen from the figure that a roughness of 0.0025 cm (0.001 in.) decreases the tendency toward separation on the lip as can be judged by the increase in the minimum local skin friction coefficient, but causes the flow to separate in the diffuser. Further increases in roughness appear to eliminate the laminar run, and move the turbulent separation point further upstream until at a roughness of 0.013 cm (0.005 in.) the turbulent separation is almost on the lip.

A small extent of roughness near the highlight may be beneficial in reducing the tendency to laminar lip separation with less adverse affect on the diffuser separation. This needs further study.

#### Effect of Scale

One of the goals of both wind tunnel model tests and theoretical calculations is to be able to predict the boundary layer behavior of full scale inlets. A step toward this goal is the use of the present program to investigate the effects on the boundary layer of changing the scale of the inlet of figure 1. Some data from this investigation are shown in figure 12 in the form of skin friction coefficient distributions. The flow conditions are such that the 30.5 cm base inlet is close to diffuser separation. If the scale is cut in half ( $D_e = 15.2$  cm) the flow separates in the diffuser. As the scale is increased through  $D_e = 61.0$  cm on up to full scale (183.0 cm) the flow becomes less likely to separate in the diffuser.

Note that the minimum  $C_f$  in the laminar region near the high-light decreases as scale increases indicating that the lip is closer to laminar separation at the larger scale. This is because at the larger size, there is a longer laminar run with a resulting thicker laminar boundary layer.

Further calculations can translate these kinds of results into the change in separation onset angle with scale. Results from preliminary calculations toward that end are shown in figure 13. Flow conditions are  $M_o = 0.18$  and  $M_T = 0.73$ ; the base  $\alpha$  is  $44^\circ$ . At these conditions the scale model ( $D_e = 30.5$  cm) is very close to separation in the diffuser; however, the full size inlet ( $D_e = 183$  cm) is a "safe" distance from diffuser separation. If  $\alpha$  is increased to  $55^\circ$  for the full size inlet, the diffuser boundary layer characteristic is hardly different from that at  $44^\circ$ ; however the lip is now very close to separation. And in fact, further calculations indicate that the lip separates at  $\alpha = 55.5^\circ$ . Reference to figure 7(b) shows that the small scale model also suffered lip separation for these flow conditions ( $M_o = 0.18$ ,  $M_T = 0.73$ ) at  $\alpha = 54^\circ$  not greatly different from  $55.5^\circ$ . Thus, for this particular case it appears that increasing the scale can improve the diffuser performance significantly but not the lip performance.

#### CONCLUDING REMARKS

The Lewis subsonic inlet programs have been used to investigate the boundary layer characteristics in an engine inlet. Comparison of calculated results with experimental data for this one inlet indicates that, when interpreted properly, the theoretical results can be used to adequately predict inlet separation bounds. The interpretation rests in hypothesizing the existence of two types of diffuser separation, termed here stable and unstable. Unstable separation is defined to be diffuser separation that propagates upstream to the lip. An experiment is required to test this hypothesis. Also, the present approach needs to be applied to additional inlets to hopefully establish its generality.

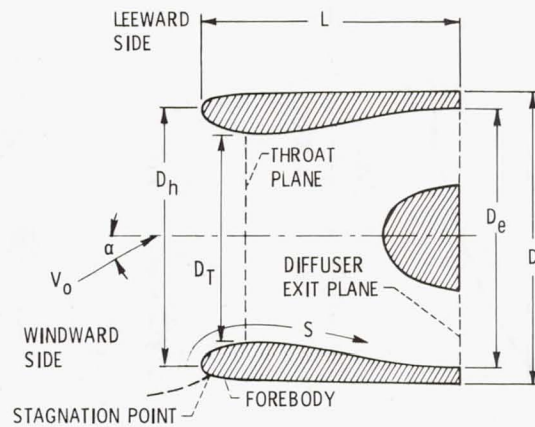
The preliminary results presented on the effects of surface roughness and scale indicate that adding lip roughness may result in a more significant improvement in boundary layer performance at larger scale than at small scale. A farther investigation of the effects of roughness and scale is needed.

The analysis technique itself could be improved in several areas: (1) incorporate shock boundary-layer interaction into the calculations, (2) provide for automatic sweep of incidence angle to determine separation onset, and (3) incorporate automatic geometry optimization techniques. These improvements should make the boundary layer program a still more accurate and useful tool for subsonic inlet design and analysis.



## REFERENCES

1. Stockman, N. O., "Potential and Viscous Flow in VTOL, STOL or CTOL Propulsion System Inlets," AIAA Paper 75-1186, 1975, Anaheim, Calif.
2. Albers, J. A. and Stockman, N. O., "Calculation Procedures for Potential and Viscous Flow Solutions for Engine Inlets," Journal of Engineering for Power, Vol. 97, No. 1, Jan. 1975, pp. 1-10.
3. Miller, B. A., Dastoli, B. J. and Wesoky, H. L., "Effect of Entry-Lip Design on Aerodynamics and Acoustics of High-Throat-Mach-Number Inlets for the Quiet, Clean, Short-Haul Experimental Engine," NASA TM X-3222, 1975.
4. Albers, J. A. and Gregg, J. L., "Computer Program to Calculate Laminar, Transition and Turbulent Boundary Layers for Compressible Axisymmetric Flow," NASA TN D-7521, 1974.
5. Herring, H. J. and Mellor, G. L., "Computer Program for Calculating Laminar and Turbulent Boundary Layer Development in Compressible Flow," NASA CR-2068, 1972.
6. Schlichting, H. (J. Kestin trans.), Boundary Layer Theory, 6th ed., McGraw-Hill, New York, 1968.
7. Felderman, E. J. and Albers, J. A., "Comparison of Experimental and Theoretical Boundary-Layer Separation for Inlets at Incidence Angle at Low-Speed Conditions," NASA TM X-3194, 1975.
8. Nikuradse, J., "Laws of Flow in Rough Pipes," NACA TM-1292, 1950.



$$\text{AREA CONTRACTION RATIO } (D_h/D_T)^2 = 1.46$$

$$D/D_e = 1.111 \quad L/D = 1$$

Figure 1. - Inlet geometry.

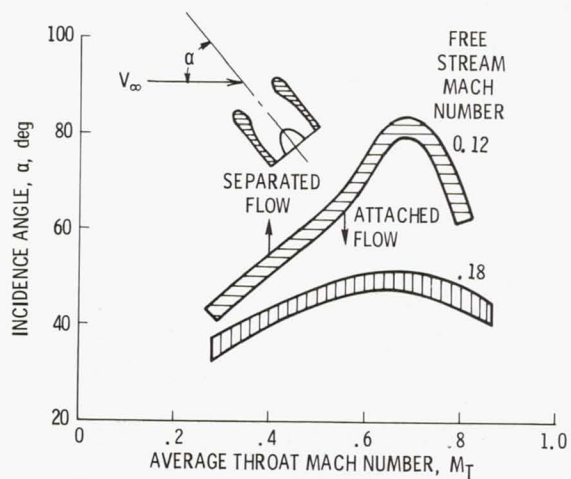


Figure 2. - Experimental variation of incidence angle at flow separation with average throat Mach number.



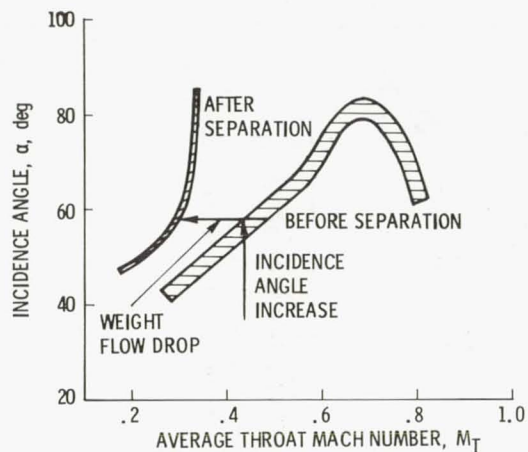
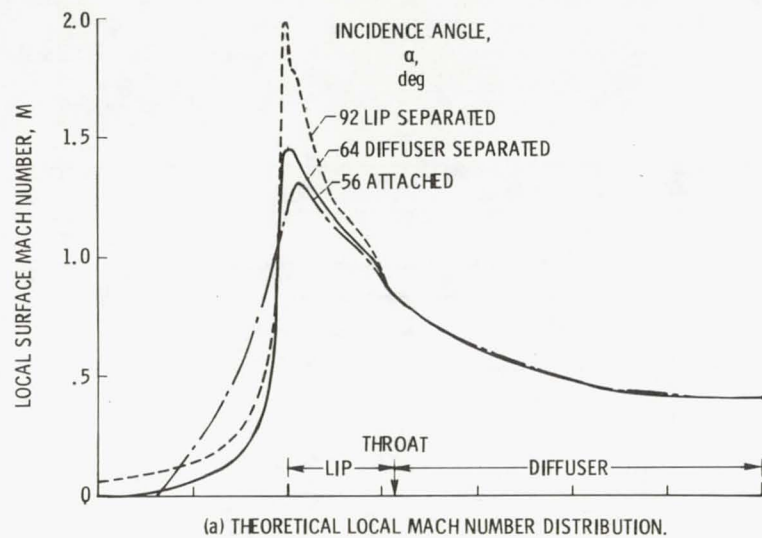
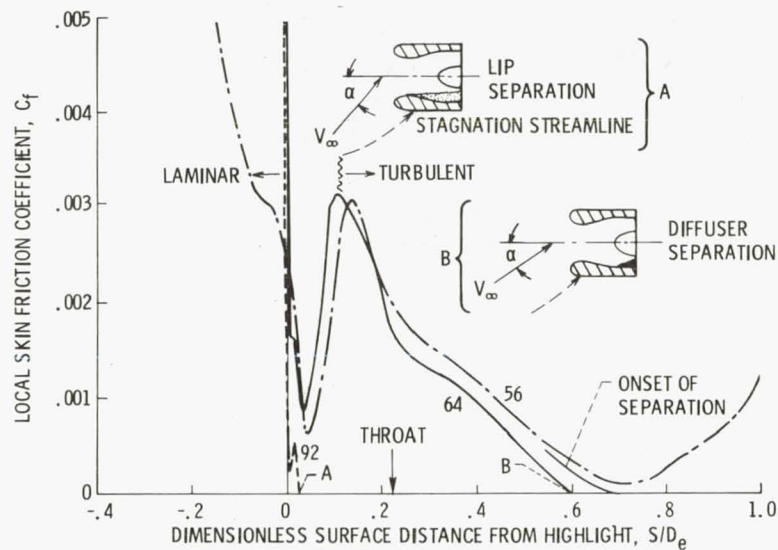


Figure 3. - Reduction of average throat Mach number due to flow separation (experimental data obtained by increasing incidence angle to point of flow separation)  $M_0 = 0.12$ .



(a) THEORETICAL LOCAL MACH NUMBER DISTRIBUTION.



(b) THEORETICAL LOCAL SKIN FRICTION COEFFICIENT.

Figure 4. - Effect of incidence angle on flow separation. Windward side of inlet.  $M_0 = 0.12$ ,  $M_T = 0.59$ .

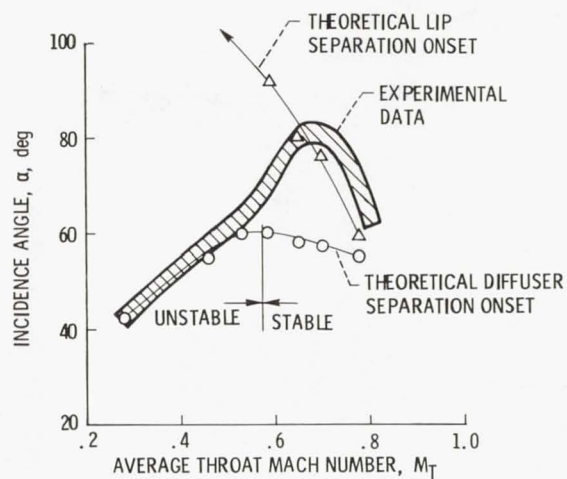


Figure 5. - Comparison of theoretical and experimental flow separation.  $M_0 = 0.12$ .

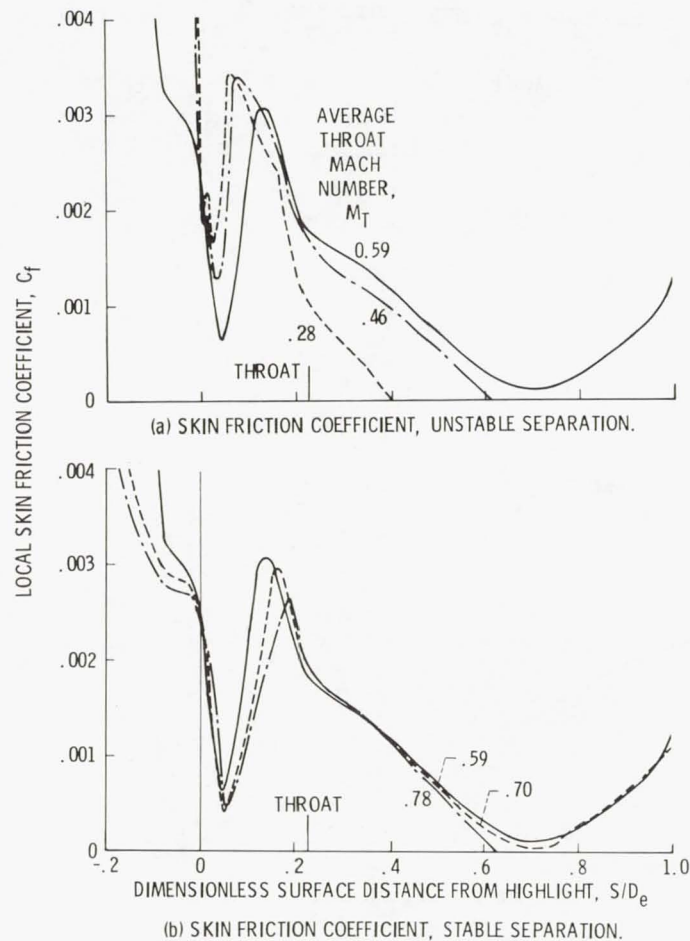
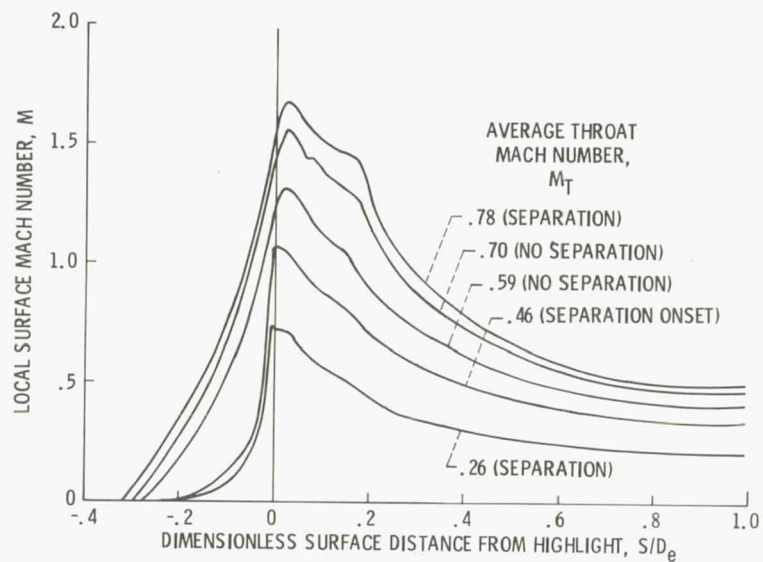


Figure 6. - Effect of average throat Mach number on location of separation. Windward side.  $M_0 = 0.12$ ,  $\alpha = 56^\circ$ .





(c) MACH NUMBER DISTRIBUTION, STABLE AND UNSTABLE CONDITIONS.

Figure 6. - Concluded.

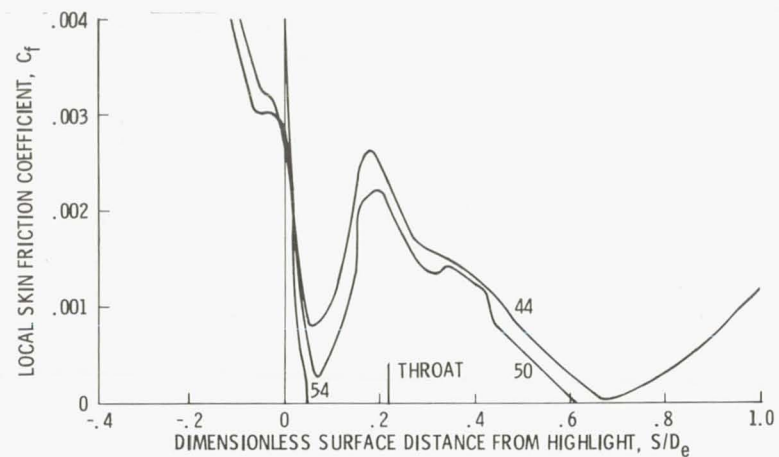
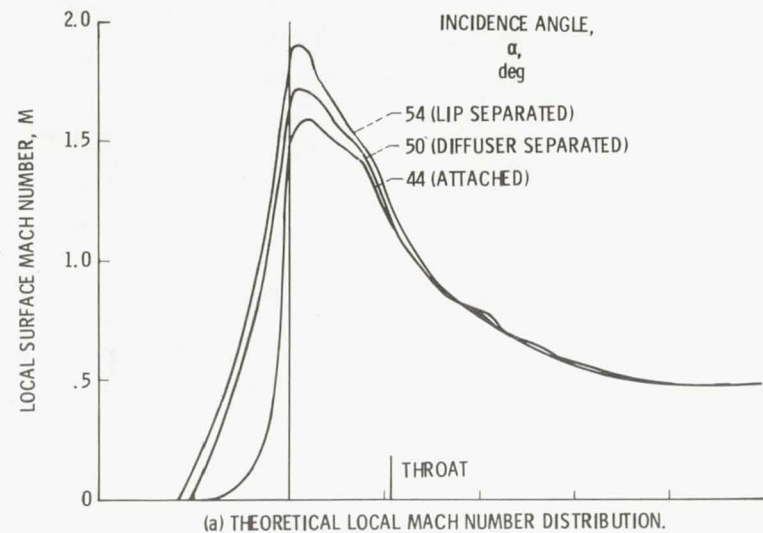


Figure 7. - Effect of incidence angle on flow separation. Windward side.  
 $M_0 = 0.18$ ,  $M_T = 0.73$ .

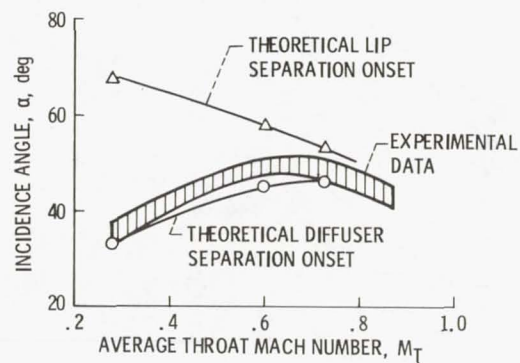
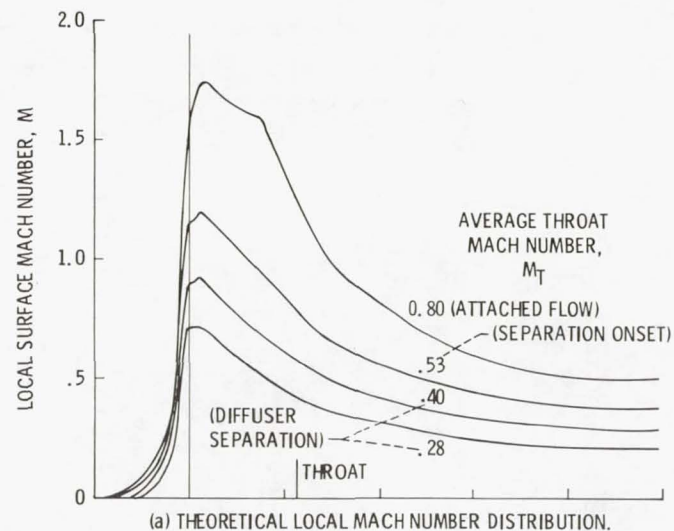
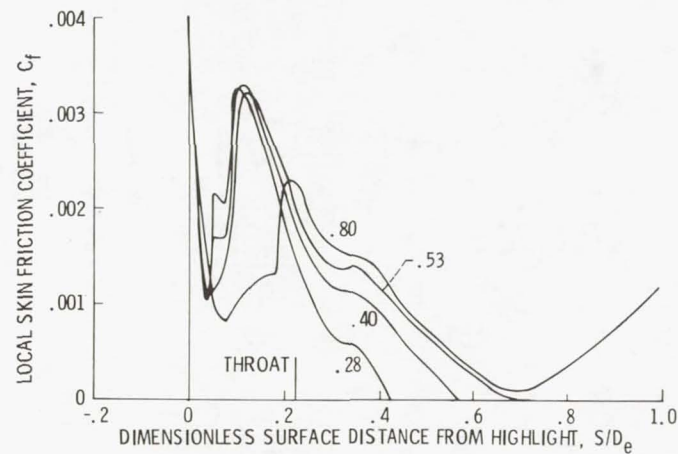


Figure 8. - Comparison of theoretical and experimental flow separation.  $M_0 = 0.18$ .



(a) THEORETICAL LOCAL MACH NUMBER DISTRIBUTION.



(b) THEORETICAL LOCAL SKIN FRICTION COEFFICIENT.

Figure 9. - Effect of average throat Mach number on local flow conditions. Windward side.  $M_0 = 0.18$ ,  $\alpha = 44^\circ$ .



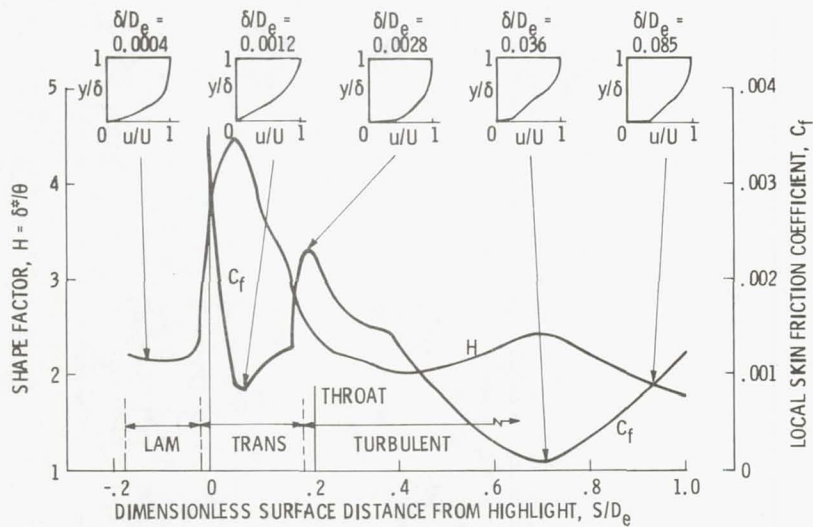


Figure 10. - Boundary layer details. Windward side.  $M_0 = 0.18$ ,  $\alpha = 44^\circ$ ,  $M_T = 0.80$ .

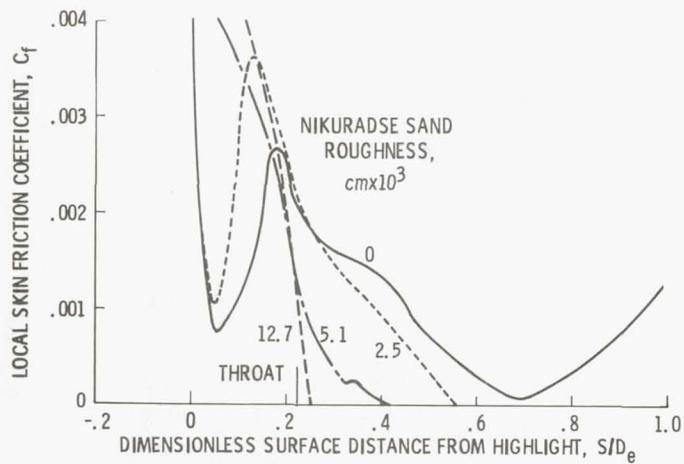


Figure 11. - Effect of surface roughness on separation. Windward side.  $M_0 = 0.18$ ,  $\alpha = 44^\circ$ ,  $M_T = 0.73$ .

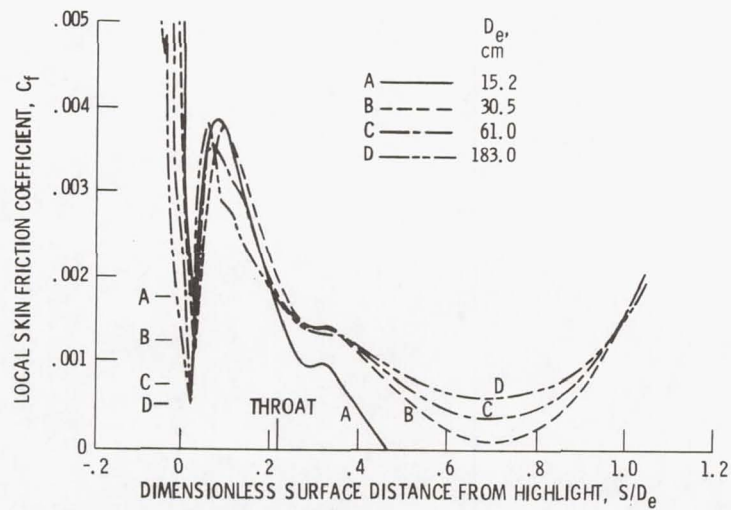


Figure 12. - Effect of scale on skin friction coefficient. Windward side of inlet.  $M_\infty = 0.13$ ,  $\alpha = 41^\circ$ ,  $M_T = 0.28$ .

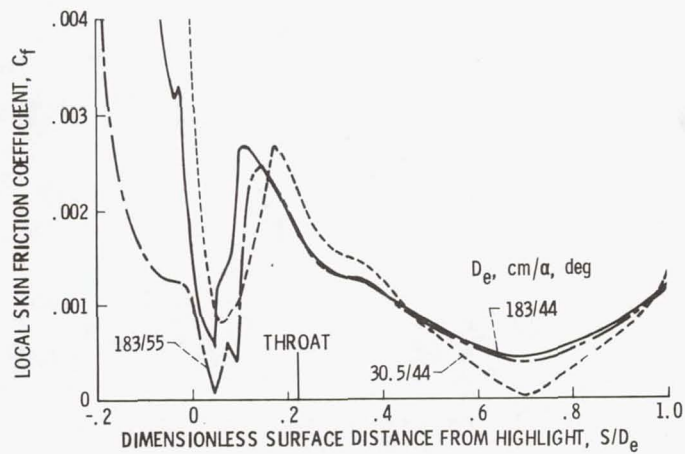


Figure 13. - Effect of scale and incidence angle on skin friction coefficient. Windward side.  $M_0 = 0.18$ ,  $M_T = 0.73$ .